Optics Communications 382 (2017) 547–555

Contents lists available at ScienceDirect

Optics Communications

journal homepage: www.elsevier.com/locate/optcom

Improved SPGD algorithm to avoid local extremum for incoherent beam combining

Guoqing Yang [a,b,*], Lisheng Liu [a], Zhenhua Jiang [a], Tingfeng Wang [a], Jin Guo [a]

[a] State Key Laboratory of Laser Interaction with Matter, Changchun Institute of Optics, Fine Mechanics and Physics, Chinese Academy of science, Changchun 130000, China
[b] University of Chinese Academy of Science, Beijing 100049, China

ARTICLE INFO

Article history:
Received 11 May 2016
Received in revised form
10 August 2016
Accepted 12 August 2016
Available online 25 August 2016

Keywords:
Laser beam combining
SPGD algorithm
Pattern recognition

ABSTRACT

The stochastic parallel gradient descent (SPGD) algorithm and the fast steering mirrors (FSM) are applied for incoherent beam combining in this paper. An equation is derived to calculate the wavefront reflected from the FSM under certain control voltages and the relationship between the strength of random disturbances and the combing efficiency is discussed via simulations, indicating that the combining efficiency is inversely proportional to the square of the strength of disturbance. The maximum value of the acceptable disturbance can be determined though the fitting curve which presents an instructional way to reduce the disturbance in advance. Besides, the SPGD algorithm is improved to overcome the weakness of tending to be trapped in the local extremum in incoherent beam combining. In the proposed algorithm, pattern recognition is used to check whether the algorithm is trapped and an "additional move" can be applied to get out of local extremum. The results of simulations show that the proposed algorithm can improve the performance of the incoherent beam combining. Comparative simulations are conducted where the value of evaluation function is increased about 60% compared to the conventional algorithm under the same conditions. The threshold of disturbance also increases about 15% when the accepted value of evaluation function set to 0.8 in the normalized form showing the feasibility of the method. Also, statistical data shows the proposed method depends less on the gain coefficient.

1. Introduction

Incoherent beam combining (ICBC) is the most promising technology to achieve high-energy laser by now [1]. ICBC has a lot of advantages like low maintenance, strong robust and compact size [2,3]. The most important issue for ICBC is the precise beam pointing under disturbances of atmospheric turbulence as well as jitter of the whole system [4]. Among all of the instruments that can be used for such scenario, the fast steering mirror (FSM) is the most proper way that can be used for its high respond speed as well as large operating frequency [5]. Besides, compare to the adaptive fiber-optics collimators (AFOC) [6–11], another device used for laser beam combining, FSM can be used in high-energy applications which is the main reason why we choose it as the combining device.

The stochastic parallel gradient descent (SPGD) algorithm can be utilized to calculate the proper control voltages applied to FSMs for precise beam overlapping. The SPGD algorithm has achieved great success since first applied to the adaptive optics area by Vorontsov in 1997 [12]. A series of improved measures have been taken to boost the speed and precision of convergence [9,12,13]. In 1998, Vorontsov proposed self-organized control structure to achieve a fast convergence. In 2000 Weyrauch proposed adaptive update gain control algorithm to enhance the adaptation speed of SPGD algorithm. Decoupled SPGD algorithm was put forward to offer fast adaptation convergence even for high-resolution adaptive optics by Vorontsov in 2002. In 2013 Geng proposed the divergence cost-function method, the divergence cost-function is proposed as a merit function for SPGD algorithm in this paper, the new merit function has a wider correction range and is free of camera's intensity-saturation than the conventional merit function like the PIB value [9], but the method to restrain the algorithm from falling in the local extremum is rarely reported. However methods to avoid local extremum are important because the algorithm would trap in the local extremum time by time when the parameters of the algorithm do not set properly or the disturbances of the system are large. In this paper a method that combines pattern recognition and SPGD algorithm is proposed to avoid the circumstance of the local extremum. Simulations are

* Corresponding author.
E-mail address: yanggq09@163.com (G. Yang).

http://dx.doi.org/10.1016/j.optcom.2016.08.028
0030-4018/

carried out to validate the feasibility of the improved algorithm. Besides, the relationship between the strength of disturbance and the local extremum is discussed and analyzed, then The disturbance's influence on the result of beam combining is analyzed.

The paper is organized as follows: Section 2 introduces the method we use to ameliorate the algorithm. Section 3 presents the simulation of the conventional algorithm as well as improved algorithm under different disturbances. At last, Section 4 gives the discussion and conclusion of the paper.

2. Improved algorithm

The most crucial problem for conventional SPGD algorithm is the selection of proper value of parameters. A large gain coefficient would lead to non-convergence and a small one would lead to low convergence speed even local extremum. A series of gain value between 0.5 and 3.5 is chosen to testify how often the SPGD algorithm would not converge. The data is showed in Table 1.

Table 1
The number of local extremum with different gain coefficients using conventional algorithm.

Gain coefficient: γ	Times stuck in local extremum	Percentage
0.5	18	90%
1	17	85%
1.5	14	70%
2	8	40%
2.5	14	70%
3	15	75%
3.5	17	85%

The conventional algorithm is tested in the optimum situation, the average J value in twenty simulations is showed in Fig. 1. Fig. 1 (a) is the times the evaluation function J appeared in the correction process. It can be seen the value in 0.58–0.60 appears the most. Fig. 1(b) is the evaluation function during the correction process and it shows the process would stuck in the local extremum clearly.

The improved algorithm combines the knowledge of the pattern recognition and the SPGD algorithm. Based on the knowledge that there will be only one light spot in the target plane when the combining process is ideal, the synopsis of the improved algorithm is listed below. A conventional CCD camera is used to acquire the configuration of the intensity distribution in the target plane and then the contour of the image can be obtained through image processing. The pattern recognition can help decide whether the correction process is stuck in local extremum through the quantity of light spots that can be detected in the contour image. An additional move will be taken when algorithm detects there are more than one light spot. Then the local extremum can be avoided.

The steps of the improved SPGD algorithm can be described as:

1) Set a group of initial control parameters $\{c_i\}$.
2) Generate a group of small perturbations $\{\delta c_i\}$ that satisfy the Bernoulli probability distribution with zero mean.
3) Apply the perturbations on the control parameters to get the evaluation functions $J(c_1+\delta c_1, c_2+\delta c_2, \ldots, c_N+\delta c_N)$ and $J(c_1-\delta c_1, c_2-\delta c_2, \ldots, c_N-\delta c_N)$
4) Evaluate the gradient using the approximate formula and update the control parameters by:
$c_i^{(n+1)} = c_i^{(n)} + \gamma \delta c_i [J(c_1+\delta c_1, c_2+\delta c_2, \ldots, c_N+\delta c_N) - J(c_1-\delta c_1, c_2-\delta c_2, \ldots, c_N-\delta c_N)]$, $i=1,2,\ldots,N$
where the n stands for the iterative number and the γ represents the gain coefficient of the SPGD algorithm.
5) Testify whether the algorithm is stuck in local extremum through pattern recognition. If the algorithm is stuck, go to step 6, if not, go to step 7.
6) Modify the gain coefficient through the “additional move”.
7) If the control parameters don't satisfy the requirement, go to step 2 to repeat the step 2 to step 6.

The evaluation function J can be chosen from the sharpness function, power in the bucket (PIB) value or other functions that converge to extremum when the correction process is done. The normalized maximum value of the intensity in the target plane is chosen as the evaluation function here. The intensity distribution captured by the camera changes to the bi-level image and then converts to the contour image using the threshold quantity that we set ahead. The process is showed in Fig. 2. The simulations below utilize six laser beams for ICBC and the parameters set in the simulations are laid out in Table 2.

The intensity distribution of six light spots shown in Fig. 2(a) is influenced by a set of disturbances caused by random jitter of the system, four of which are gathered together and the rest two spots have strong fluctuations that lead to a trip-out of the main spot. Bi-level image can be obtained through a proper threshold as we showed in Fig. 2(b), (d) and (f). The threshold quantity here is the gray-level value. Each light spot may not be visualized in the contour image as showed in Fig. 2(e) when the quantity is too small as we use in Fig. 2(b). Also some light spots may be disappeared in Fig. 2(g) when the quality we use is too big. The proper gray-level value is set to 9 in the simulations as showed in Fig. 2(c) according to the strength of one light spot, and the contour extraction result showed in Fig. 2(f) indicates that every light spot can be identified clearly. The selection of threshold is a tricky problem for the algorithm. In this paper, the selection of the threshold is performed through measuring the gray-level value of each light spot in advance. The proper threshold is proportioned to the maximum gray-level value with a coefficient a (a is 0.8 in this paper). When the values of certain closed curve in the target plane are bigger than the threshold, it is believed that there is a light spot inside the curve. As contrary, the gray value which is smaller than the threshold is some flares due to the turbulence as well as diffraction.

The pattern recognition [14] can be applied to identify the quantity of light spots in the contour image. The result is showed in Fig. 3.

When the number of the circles is larger than 1 after a sequence of correction procedures, it can be confirmed that the algorithm is stuck in the local extremum, the "additional move" is taken and then the algorithm can be executed continually.

The "additional move" this paper taken is increasing the value of the gain coefficient. It can be inferred from the research of SPGD algorithm that a large gain coefficient can lead to non-convergence and a small one will cause slow convergence speed. The select of a gain coefficient is done by experience for there are no efficient methods for choosing proper gain coefficient so far. Weyrauch and his team proposed the adaptive coefficient method, but the value of the update function $H^{(n)}$ is very difficult to determined. The gain should be related to the evaluation function, it has a large value when the evaluation function is small (for the evaluation function in this paper) and becomes smaller when the evaluation function changes during the correction process. The coefficient is set to be the form showed in Eq. (1) in this paper where the α is the update coefficient with a value less than 1 and J is the value of the evaluation function used in this paper. The superscript n is the iterative number when the system makes sure the algorithm is stuck in the local extremum.

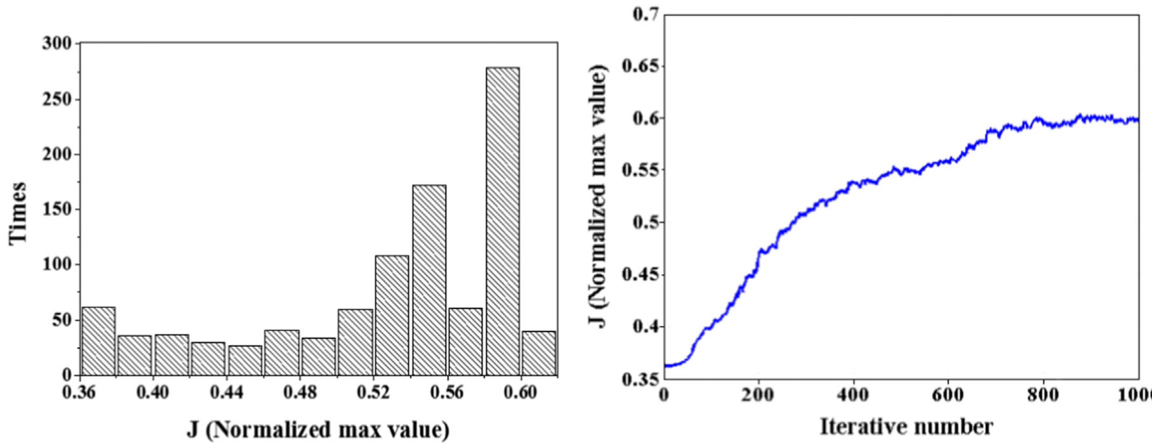

Fig. 1. (left) The times that the *J* appeared in the correction process; (right) The average of *J* during the correction process.

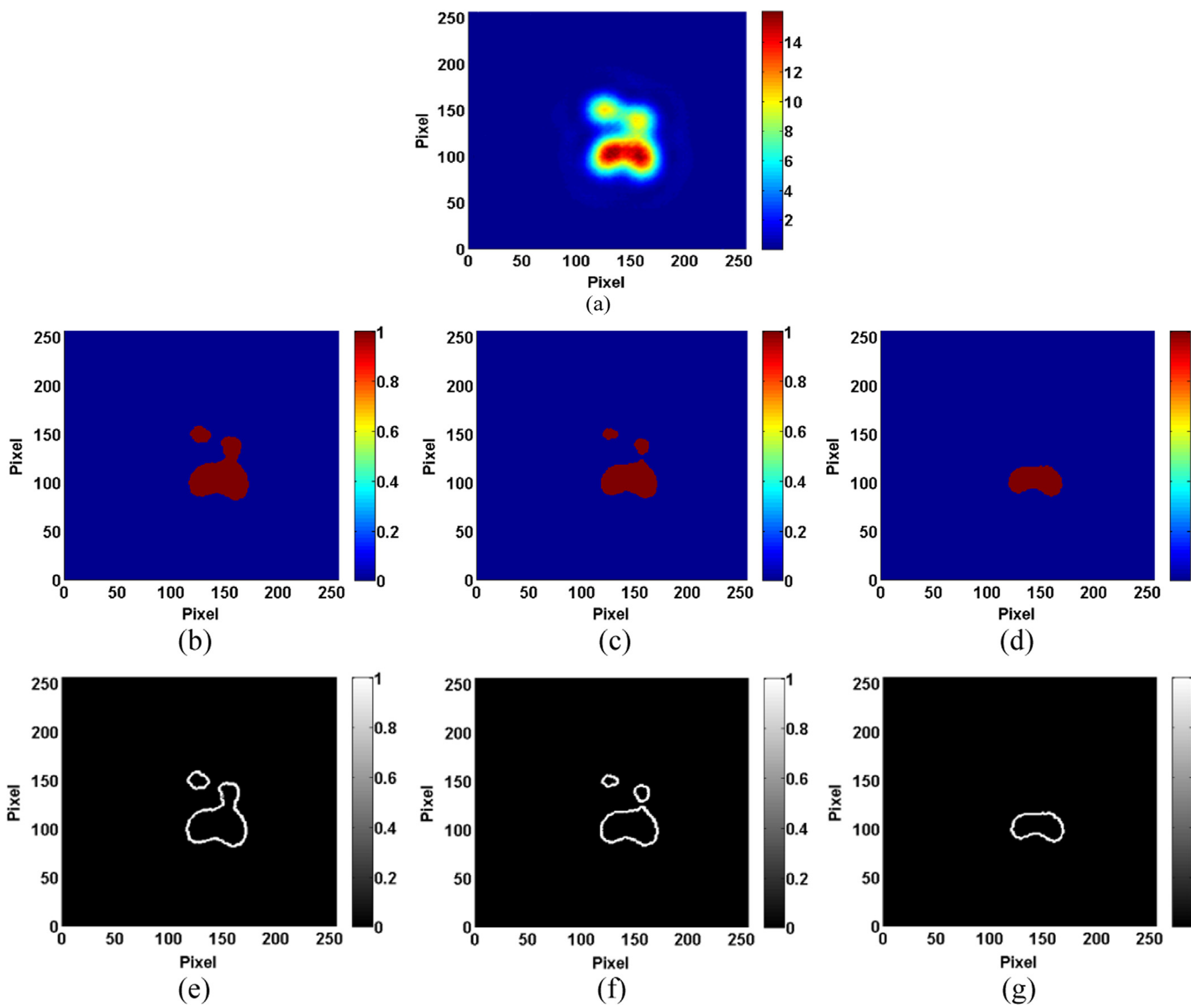

Fig. 2. The process of the intensity distribution in the target plane changes to the bi-level image and the contour image using different threshold quantity; (a) Intensity distribution; (b), (c), (d) Bi-level image with threshold quantities of 8, 9 and 10; (e), (f), (g) Corresponding contour images with (b), (c) and (d).

Table 2
The main parameters used in simulations.

Parameter	Value
Propagation distance: L	300 m
Wavelength: λ	1064 nm
Beam waist: ω_0	0.017 m
Radius of the FSM: r	0.007 m
Sampling number: N	256
Coherent length of atmosphere: r_0	0.1 m

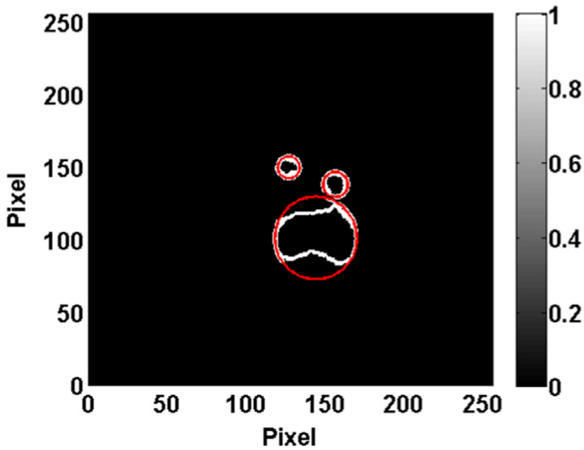

Fig. 3. The contour image after pattern recognition. Every part is enveloped by a red circle, the number of the spots can be calculated by summing the circles.

$$\gamma^{(n+1)} = 2\gamma^{(n)} + \alpha\left(\frac{1}{J^{(n)}} - \gamma^{(n)}\right) \tag{1}$$

3. Verification of the proposed algorithm

3.1. Model for ICBC

The optical setup used in this paper is showed in Fig. 4 and the distribution of six FSMs is showed in Fig. 5(a) in which d is the diameter of the FSM and $D=3d$ is the diameter of the incident plane. Each mirror has 4 actuators mounted at the distance of $0.464d/2$ in two orthogonal directions.

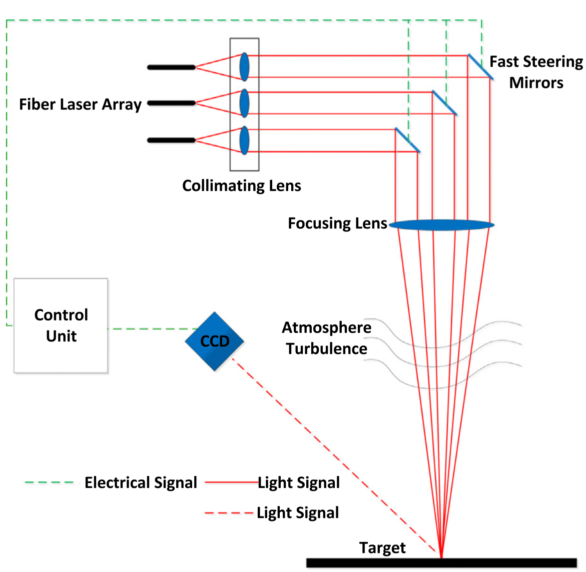

Fig. 4. The optical setup of the ICBC. The camera would be used with a telescope or something that can image the intensity into the camera. The signal captured by the camera will be sent to the control unit where it would be analyzed and then produce a series of control voltages applied to the FSMs.

We assume that the reflective mirror of the FSM is rigid. And then the relationship between the reflect beam and the control voltage can be deduced by the knowledge of geometric optics [15] as showed in Eq. (2).

$$A_r = a_0 \exp\left[\frac{-\left(x^2+y^2\right)}{2w_0^2}\right] \times \exp\left[ik\left(x\cos\left(\frac{\pi}{2}+2\theta_x\right) + y\cos\left(\frac{\pi}{4}+\sqrt{2}\theta_y\right) + z\cos\left(\frac{\pi}{4}\right)\right)\right] \tag{2}$$

In Eq. (2), the initial laser beam is the Gaussian beam, a_0 and w_0 are the amplitude and beam waist of the initial Gauss beam separately. θ_x and θ_y represent the tilt angles that the mirror has in two directions under the control voltages V_x and V_y, s_0 is the displacement of the FSM when a unit voltage is applied. The relationships between the displacement and the control voltages are expressed in Eq. (3) and Eq. (4).

$$\cos(\theta_x) = \frac{s_0}{0.464r\sqrt{1+\left(\frac{s_0}{0.464r}\right)^2\left(V_x^2+V_y^2\right)}}|V_x| = \frac{s_0}{\sqrt{(0.464r)^2 + s_0^2\left(V_x^2+V_y^2\right)}}|V_x| \tag{3}$$

$$\cos(\theta_y) = \frac{s_0}{0.464r\sqrt{1+\left(\frac{s_0}{0.464r}\right)^2\left(V_x^2+V_y^2\right)}}|V_y| = \frac{s_0}{\sqrt{(0.464r)^2 + s_0^2\left(V_x^2+V_y^2\right)}}|V_y| \tag{4}$$

Then the laser beam will propagates through atmospheric turbulence and reaches the target plane as showed in Fig. 4.

3.2. Simulations using conventional algorithm

In the real applications, all of the sources of disturbance have the dynamic characteristics, so it will be necessary to consider the dynamic characteristic when validate the feasibility of the proposed algorithm. In the simulation, a series of random jitter that satisfy the Gaussian distribution with the mean value of 0 is added to the whole system, besides, the dynamic turbulence is simulated using Taylor's hypothesis of frozen turbulence which indicates the temporal variations of meteorological quantities at a point are produced by advection of these quantities by the mean wind speed flow and not by changes in the quantities themselves. So a series of phase screens with large pixels are simulated and move along a direction in order to simulate the dynamic characteristic of the turbulence. The parameters for generating turbulence like the coherent length and the size of phase screen are set to be equal among all the simulations, but the phase screens would be refreshed for each simulation. The evaluation function during the correction process is illustrated in Fig. 6. In this paper, the maximum value of the intensity in the target plane is chosen as the evaluation function J. The value of evaluation function in the correction process is normalized by dividing the maximum value when the ICBC is ideal. The analytical form of J is shown in Eq. (5). I_0 is the distribution of intensity when the combing process is ideal.

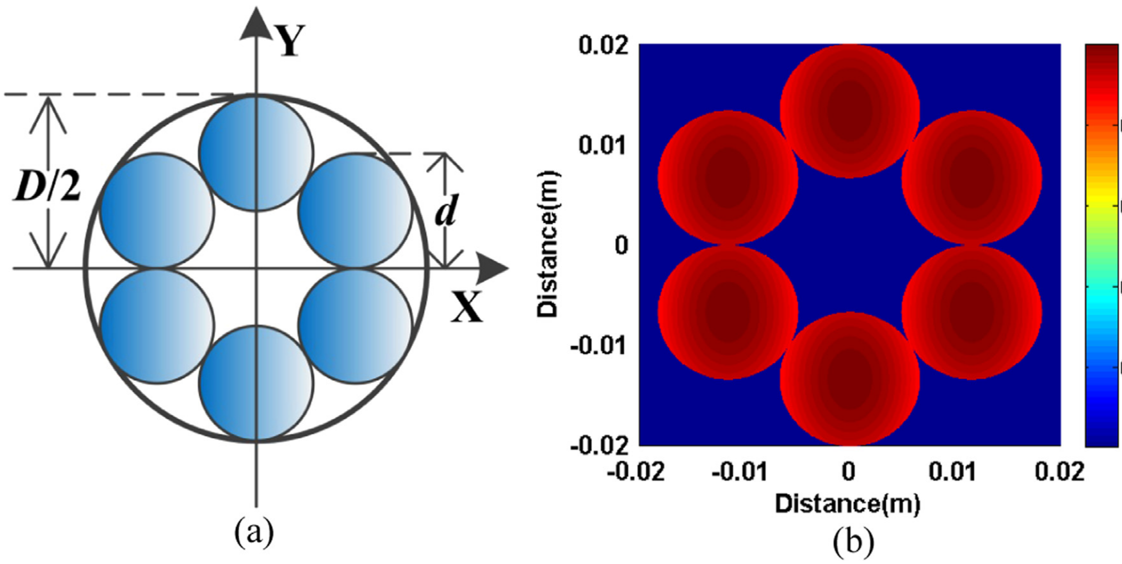

Fig. 5. (a) The distribution of six FSMs; (b) the initial Gauss beams in the incident plane.

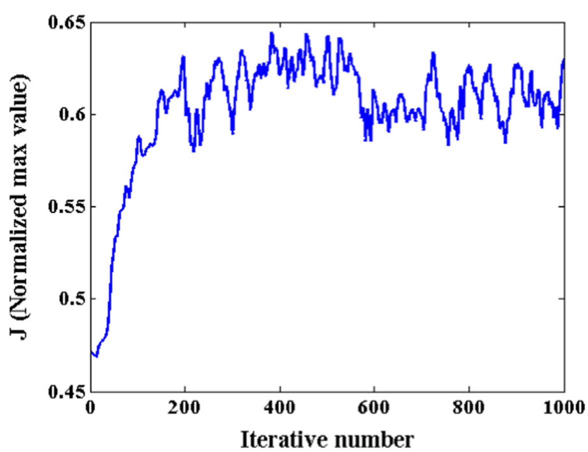

Fig. 6. The normalized evaluation function J changes in a correction process that stuck in local extremum.

$$J = \max(I)/\max(I_0) \tag{5}$$

The max value is about 0.5 when the process is steady, indicating the algorithm is stuck in local extremum.

The intensity distribution in the target plane for this process is illustrated in Fig. 7. The light spots showed in Fig. 7(a) can not gather as one spot because of the random jitter of the system. The intensity distribution in Fig. 7(b) shows a good correction result, however, there is still one light spot on the side of the main spot and it cannot be corrected using conventional algorithm.

The final average value of evaluation function J is influenced by the strength of the random jitter of the system is going through. The strength of random jitter of the system is set to be 0.4, 0.5, 0.6, 0.75, 1 (in the normalized form, the max disturbance is set to be 1 here). The simulations are carried out under the above disturbances. For each time, ten simulations are performed and the value of the evaluation function J is averaged over all of ten simulations. When the correction is steady, the relationship curve between the value of J and the strength of random jitter is showed in Fig. 8(a). The fitting function can be expressed as Eq. (6).

$$J = 1.377x^2 - 2.805x + 1.798 \tag{6}$$

It can be inferred from Eq. (6) that the efficiency of correction decreases as the disturbance grows, the system would never satisfy the need of application unless the strength of disturbance is weak enough. J=0.8 is set to be the minimum accepted value of

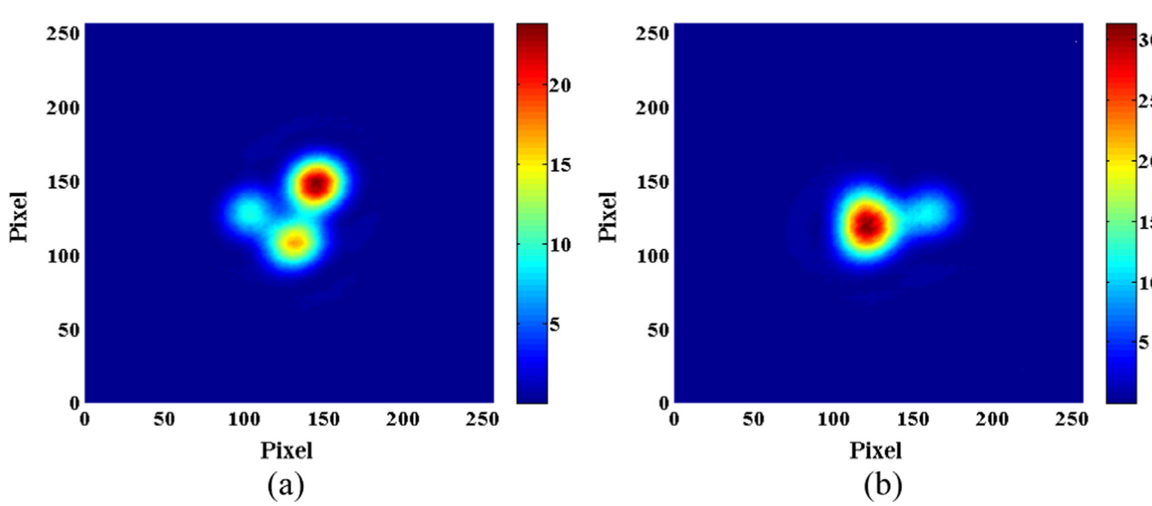

Fig. 7. The intensity distribution in the target plane under the correction using conventional algorithm. (a) Initial intensity distribution; (b) Intensity distribution after correction.

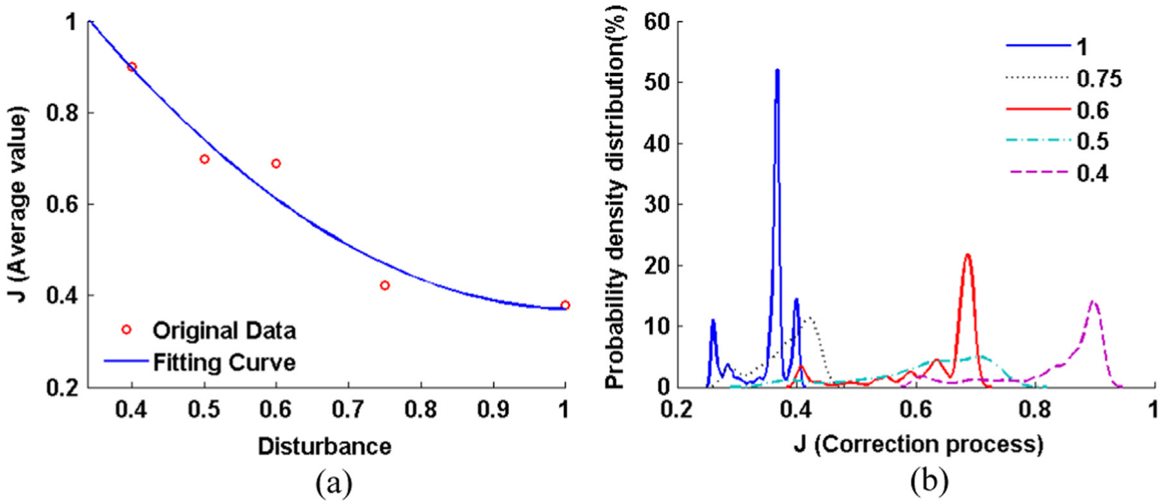

Fig. 8. (a) The relationship between J and strength of disturbance, the blue curve represents the fitting curve of the relationship and the red circles stand for the value the simulation got; (b) The probability distribution of evaluation function J during the correction process under different strengths of disturbance. (For interpretation of the references to color in this figure legend, the reader is referred to the web version of this article.)

the correction process, and then the Eq. (6) can be applied to calculate the strength of disturbance. The result is 0.46 (in the normalized form).

Fig. 8(b) shows the probability distribution of J under different disturbances. The purple line stands for the weakest disturbance has a wider distribution and a greater probability to a better correction result.

3.3. Simulations using improved algorithm

The improved algorithm is applied in this section. The parameters used here are exactly the same parameters used in Section 3.2. The recognition takes place after the iterative number is larger than 100 which is the time when the correction process becomes steady as showed in Fig. 6. The strength of disturbance set here is 0.6 (in the normalized form as Section 3). A serial of simulations are performed to find out the optimum value of the update coefficient α in Eq. (1) in advance. The update coefficient α is set to be 0.04 in the following simulation. Fig. 9(a) is correction process using improved algorithm under the same conditions like in Fig. 5. It can be seen from Fig. 9(a) that the correction process has some points at which the evaluation function J would increase abruptly, that is because the additional move is taken at these points.

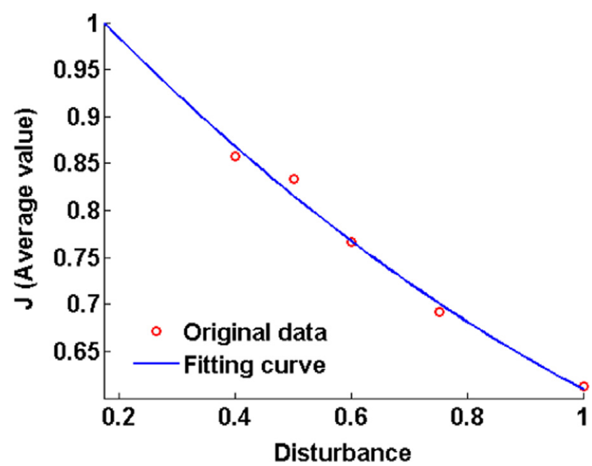

Fig. 10. The relationship between J and strength of disturbance under the condition of proposed algorithm, the blue curve represents the fitting curve of the relationship and the red circles stand for the value the simulation got. (For interpretation of the references to color in this figure legend, the reader is referred to the web version of this article.)

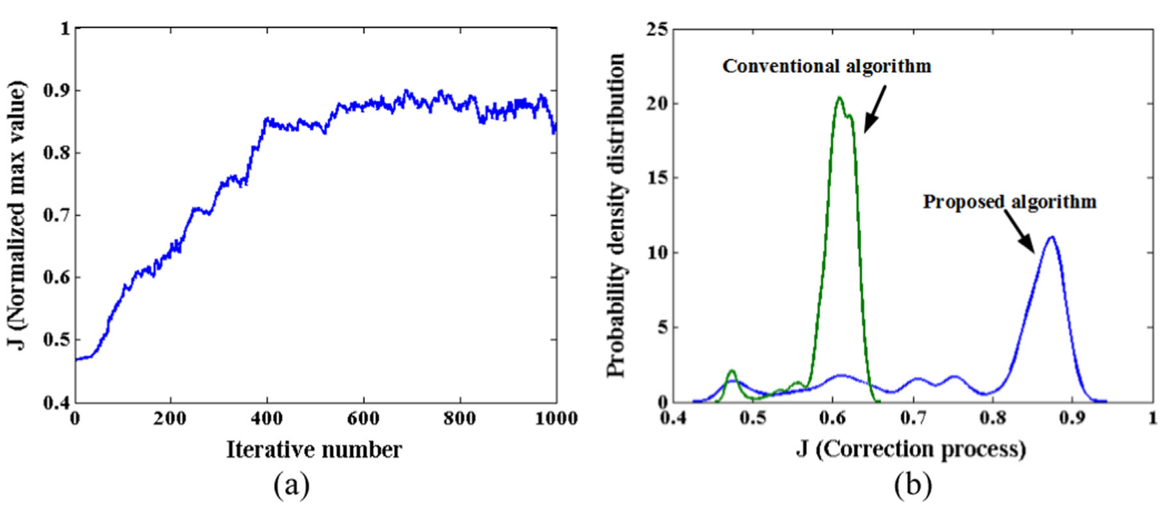

Fig. 9. (a) The normalized evaluation function J changes in a correction process without local extremum; (b) The probability distributions of conventional algorithm and proposed algorithm under the same external conditions. (For interpretation of the references to color in this figure, the reader is referred to the web version of this article.)

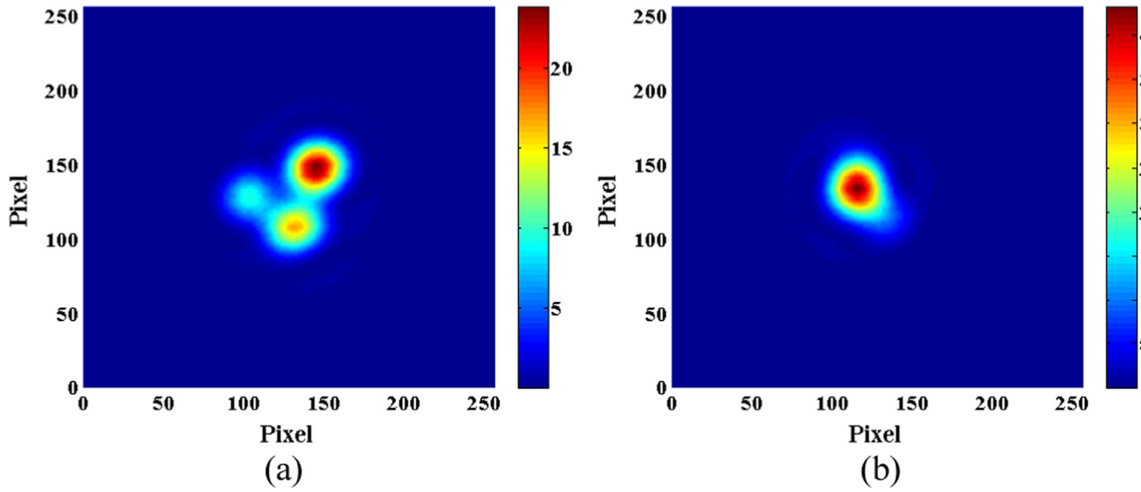

Fig. 11. The intensity distribution in the target plane under the correction using improved algorithm. (a) Initial intensity distribution; (b) Intensity distribution after correction.

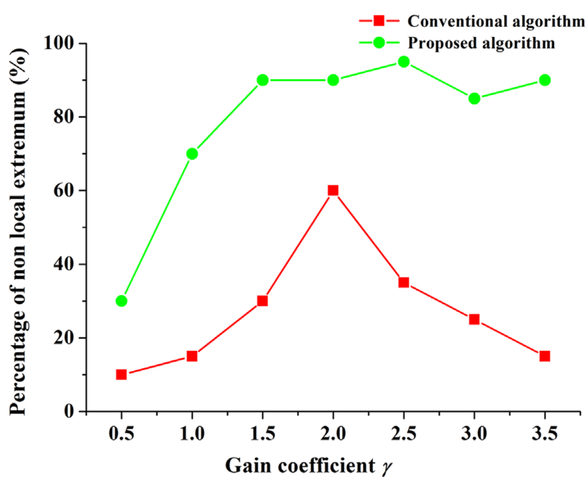

Fig. 12. Percentage of non-local extremum under different gain coefficient in conventional algorithm and proposed algorithm. (For interpretation of the references to color in this figure, the reader is referred to the web version of this article.)

Without the abrupt jumps, the correction process would stuck in the local extremum according to the tendency showed in Fig. 9(a). This phenomenon indicates the improved algorithm can help the correction process get out of the local extremum efficiently.

Compared to data showed in Fig. 6, the value of J when the process becomes steady is increased about 60%. Fig. 9(b) shows the probability distributions of correction using conventional algorithm and proposed algorithm. The green line representing the proposed algorithm has a wider distribution among the value of evaluation function and a larger most possible value about 0.8 which indicate the feasibility of the proposed algorithm.

The disturbances are also set to be 0.4, 0.5, 0.6, 0.75, 1 here, the number of simulation under a certain disturbance is also 10. The relationship between the average value of J and the strength of disturbance of the proposed algorithm is also discussed here, showed in Fig. 10.

The fitting curve is expressed in Eq. (7). The curve decreases slower compared to the one showed in Fig. (a). J=0.8 is also tested using Eq. (7), the answer we got is about 0.53, increased about 15% compared to the result in Eq. (6).

$$J = 0.1832x^2 - 0.6872x + 1.113 \tag{7}$$

The distribution of intensity in the target plane after correction is showed in Fig. 11. The initial condition is same with Fig. 7. It can be seen the proposed algorithm achieves very promising result.

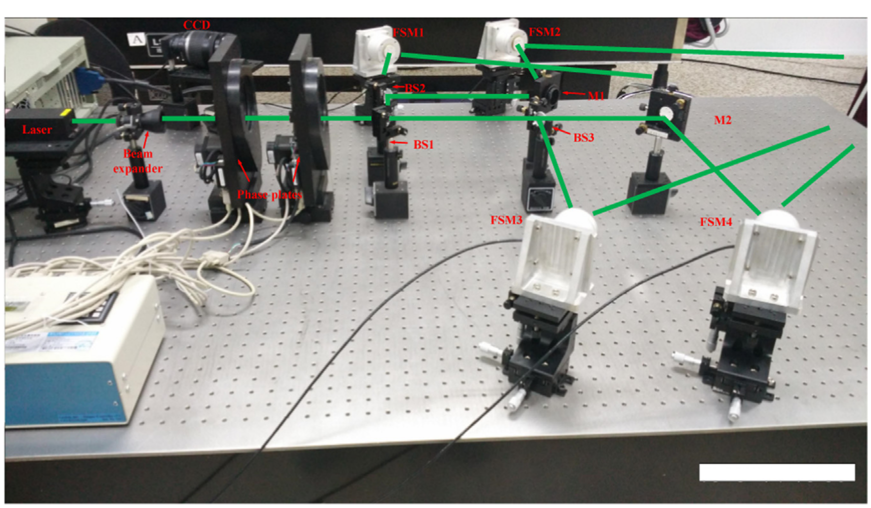

Fig. 13. Experimental setup for combining four laser beams using the proposed algorithm. BS stands for the beam splitter, M1 and M2 are conventional reflecting mirrors. The laser beam propagates through a pair of phase plates. The BS1 split the beam, then each beam is split individually by BS2 and BS3. The four laser beams would be reflected by the FSMs. The intensity distribution on the target plane is acquired by the CCD camera.

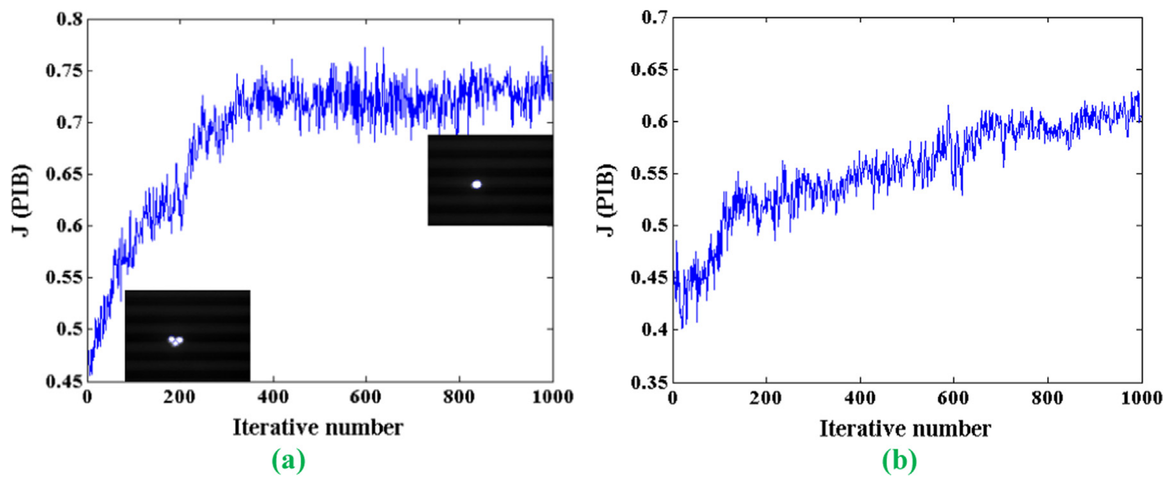

Fig. 14. Experimental result of four laser beams combining. (a) The PIB value during the correction process using the improved algorithm; (b) The PIB value during the correction process using the conventional algorithm.

Compared to Fig. 7(b), the light spot that cannot be corrected disappeared, the improved algorithm solve the problem of local extremum. Fig. 12 is the percentage of non-local extremum in the proposed algorithm as well as conventional algorithm. Under each gain coefficient, the simulation is performed twenty times. Red line (conventional algorithm) has the most proper value of gain coefficient γ. Neither a larger or a smaller one would achieve a excellent performance. However the proposed algorithm has promising result among a wider distribution of γ and the percentage of non-local extremum is larger than the conventional algorithm. This character allows us to choose the initial gain coefficient in a loose form.

The proposed algorithm can improve the performance of ICBC system utilizing SPGD algorithm, it can be used to avoid local extremum which the conventional algorithm would fall into. The algorithm is readily implemented in hardware. Besides, the proposed algorithm would be used in other areas that need correction of multiple beams. However the proposed algorithm still faces some problems, the processes of image processing and pattern recognition cost time and the update coefficient α can't be determined through analytical method, if the parameters for ICBC change, the value of α can only be determined through a lot of simulations and that makes the experiment very difficult to carry out in the real applications.

3.4. Experiment

An simply experiment that combines four laser beams using the proposed algorithm is performed. The experimental setup is showed in Fig. 13.

The result of the experiment is illustrated in Fig. 14(a). The evaluation function fluctuates a lot due to the dynamic turbulence the phase plates introduce. The phase plates is rotating when the experiment is carried out. The dynamic error can be generated through the rotating plates. Different rotating speed indicates different strength of the turbulence. The vibration showed in Fig. 14(a) indicates the phase plates is sufficient for simulating the dynamic errors. However the result is promising which has significantly increased the PIB. The image shown in the left bottom of Fig. 14(a) is the intensity distribution the CCD acquired in the beginning of the correction process. The image in the right upside is the intensity distribution when the correction process is done. It can be inferred from the two images that the proposed algorithm can achieve promising result. The result showed in Fig. 14(b) is the correction process using the conventional algorithm. The PIB of the intensity distribution is about 0.6 when the correction is done which is smaller than the PIB showed in Fig. 14(a). It can be inferred from Fig. 14 that the improved algorithm can get out of the local extremum efficiently. The feasibility of the improved algorithm is verified.

When the algorithm is applied in the real applications, the frame rate of the conventional commercial CCD is far below the bandwidth of the proposed algorithm which can up to thousands Hz like the SPGD algorithm. However the tip-tilt component of the turbulence is the main source the proposed algorithm corrects and the bandwidth of the tip-tilt component has the order of 10^1 Hz, thus making the commercial CCD available in the correction process.

4. Conclusion

The improved algorithm of SPGD is proposed in this paper. In this method, the knowledge of pattern recognition is used to verify whether or not the algorithm is stuck in the local extremum and then an "additional move" is applied to get it out. According to the simulation, the improved algorithm can increase the value of J under different strengths of disturbance. The probability density distributions under the two conditions show the effect of the improved algorithm. The relationship between average value of J and strength of disturbance is a parabola according to the fitting curves of the proposed algorithm as well as the conventional algorithm. This unique feature can help us to estimate the result of the correction and give the guidance to decrease the disturbance. An equation of changing gain coefficient is also proposed and verified in the simulation. When the strength of disturbance is 0.6 (in the normalized form), the proposed algorithm has a larger value of J which indicates a better correction result. The result of ICBC using proposed algorithm is presented, which shows the validity and the feasibility of the algorithm in the area of ICBC. Besides, the proposed method allows to choose the initial gain coefficient in a wider range. Therefore, it is worthy to study and apply the proposed algorithm for its advantages.

Acknowledgments

The study is sponsored by the National Nature Science Foundation of China (Grant no. 61205143).

References

[1] H. Injeyan, G.D. Goodno, High Power Laser Handbook, Mcgraw-Hill Publ. Comp., New York, USA, 2011.

[2] R. Uberna, A. Bratcher, B.G. Tiemann, Power scaling of a fiber master oscillator power amplifier system using a coherent polarization beam combination, Appl. Opt. 49 (2010) 6762–6765.

[3] A.T.J. Wagner, Fiber laser beam combining and power scaling progress: air force research laboratory laser division, Proc. SPIE – Int. Soc. Opt. Eng. 8237 (2012) 1844–1864.

[4] P. Sprangle, A. Ting, J. Penano, R. Fischer, B. Hafizi, Incoherent combining and atmospheric propagation of high-power fiber lasers for directed-energy applications, Quantum Electron. IEEE J. 45 (2009) 138–148.

[5] A. Kudryashov, A. Alexandrov, A. Rukosuev, V. Samarkin, P. Galarneau, S. Turbide, F. Châteauneuf, Extremely high-power CO_2 laser beam correction, Appl. Opt. 54 (2015) 4352–4358.

[6] L. Liu, M.A. Vorontsov, E. Polnau, T. Weyrauch, L.A. Beresnev, Adaptive phase-locked fiber array with wavefront phase tip-tilt compensation using piezoelectric fiber positioners, in: Optical Engineering+ Applications, (International Society for Optics and Photonics), 2007, 67080K-67080K-67012.

[7] M.A. Vorontsov, T. Weyrauch, L.A. Beresnev, G.W. Carhart, L. Liu, K. Aschenbach, Adaptive array of phase-locked fiber collimators: analysis and experimental demonstration, Sel. Top. Quantum Electron. IEEE J. 15 (2009) 269–280.

[8] X. Wang, X. Wang, P. Zhou, R. Su, C. Geng, X. Li, X. Xu, B. Shu, 350 W coherent beam combining of fiber amplifiers with tilt-tip and phase-locking control, Photonics Technol. Lett. IEEE 24 (2012) 1781–1784.

[9] C. Geng, W. Luo, Y. Tan, H. Liu, J. Mu, X. Li, Experimental demonstration of using divergence cost-function in SPGD algorithm for coherent beam combining with tip/tilt control, Opt. Express 21 (2013) 25045–25055.

[10] D. Zhi, P. Ma, Y. Ma, X. Wang, P. Zhou, L. Si, Novel adaptive fiber-optics collimator for coherent beam combination, Opt. Express 22 (2014) 31520–31528.

[11] F. Li, C. Geng, X. Li, Q. Qiu, Co-aperture transceiving propagation of two combined laser beams based on adaptive fiber coupling control, Photonics Technol. Lett., IEEE (2015), PP, 1-1.

[12] M.A. Vorontsov, G.W. Carhart, J.C. Ricklin, Adaptive phase-distortion correction based on parallel gradient-descent optimization, Opt. Lett. 22 (1997) 907–909.

[13] K. Wu, Y. Sun, Y. Huai, S. Jia, X. Chen, Y. Jin, Multi-perturbation stochastic parallel gradient descent method for wavefront correction, Opt. Express 23 (2015) 2933–2944.

[14] R.C. Gonzalez, R.E. Woods, S.L. Eddins, Digital Image processing using MATLAB (Pearson Education India), 2004.

[15] M. Born, E. Wolf, Principles of Optics, with contributions by A.B. Bhatia, P.C. Clemmow, D. Gabor, A.R. Stokes, A.M. Taylor, P.A. Wayman, W.L. Wilcock, ISBN 0521642221. Cambridge, UK: Cambridge University Press, October 1999, pp. 986.